# $Li_4Ti_5O_{12}$ on Graphene for High Rate Lithium Ion Batteries

**Lei Wen,[a] Ji Liang,[a] Cheng-Ming Liu,[a] Jing Chen,[a] Quan-guo Huang,[b] Hong-ze Luo,[c] and Feng Li[a,z]**

[a]*Shenyang National Laboratory for Materials Science, Institute of Metal Research, Chinese Academy of Science, Shenyang 110016, People's Republic of China*
[b]*Deyang Carbonene Technology Co., Ltd., Deyang 618000, People's Republic of China*
[c]*Council for Scientific and Industrial Research, Pretoria 0001, South Africa*

Spinel $Li_4Ti_5O_{12}$ has been considered as a promising anode material to substitute graphite in lithium ion batteries (LIBs) for large scale electrical energy storage due to its high safety and long cycling stability. However, the drawback of its poor rate performance still hinders it from wide practical application. In this study, with the aim to solve this issue, we have designed a wrinkled graphene layer between the active spinel $Li_4Ti_5O_{12}$ and aluminum current collectors by a blade coating method. This introduced wrinkled graphene layer provides larger contact area, lower contact resistance, stronger adhesion and better electrode stability of $Li_4Ti_5O_{12}$ electrode. As a result, the rate performance of spinel $Li_4Ti_5O_{12}$ has been significantly improved, without compromising its other properties.



Manuscript submitted August 9, 2016; revised manuscript received September 29, 2016. Published November 3, 2016.

Spinel $Li_4Ti_5O_{12}$ (LTO) has a lithium intercalation potential of 1.55 V vs. lithium with a theoretical capacity of 175 mAh $g^{-1}$. Due to its high thermal stability, superior safety, and long cycle life, LTO has been considered as a very promising alternative anode material to replace graphite in lithium ion batteries (LIBs), for large-scale storage of electricity, e.g. hybrid electric vehicles and grid-scale renewable energy plants at low costs.[1–3] However, the drawback of its poor rate performance, which originates from its intrinsic low electronic conductivity, still severely hinders it from being widely and practically applied. In order to improve the rate performance of LTO, strategies have been developed, mainly aiming at enhancing the electronic and ionic conductivity of LTO. These include: reducing LTO particle size,[4–6] coating LTO by conductive carbon,[7–10] and doping LTO at Li and Ti sites with heteroelements.[11–13] Although they could enhance the rate capability of LTO to a certain extend, many obstacles still remain to prevent it from being commercially deployed. For example, nano-sized or carbon-coated LTO can effectively improve the rate performance of LTO, however, these methods usually result in low tap density, low thermodynamic stability, detrimental surface-reactions, and/or high cost, resulting in lowered volumetric energy densities and/or other issues for practical applications.[14,15] Another critical yet under-estimated aspect that possibly influences the facileness of electron transportation is the interface contact between LTO and Al. During manufacturing of LTO-based electrode, the active material (LTO), combined with conductive additive (i.e. carbon black) and binder (poly vinylidene fluoride, PVDF), is directly pasted onto Al foil as current collector. And the contact between the active material and the current collector is the critical factor for transport of electrons to/from the electrode, which substantially influences the overall performance of LIBs.[16,17] However, Al foil as current collectors often show weak adhesion and limited contact area to the electrode material.[18,19] Therefore, simply pasting LTO on conventional Al foil could not deliver satisfactory rate performances.[17] In order to solve this issue, a few previous works addressed that carbon coating on Al foil can reduce the contact resistance and corrosion, improving electrochemical performance.[18,20] However, the conventional carbon coating (such as carbon black and graphite powder) cannot cover the Al foil to form a continuous, ultrathin, and rugged surface.

Graphene, a two-dimensional nanosheet composed of $sp^2$-hybridized carbon atoms, has high electronic conductivity and attractive mechanical properties, which is regarded as an ideal conductive additive for LIBs.[21–23] By using graphene to form a conductive network throughout the LTO nanoparticles, the rate performance of LTO can be improved.[24,25] However, in the previous studies, graphene often tends to agglomerate due to strong π-π and van der Waals interactions. Consequently, it is very hard to effectively disperse graphene among the LTO particles to form the ideal mono-disperse structure.

In this work, we propose an alternative route by simply introducing a wrinkled graphene layer into the conventional electrode configuration between the LTO and Al foil to improve the rate performance of LTO materials. In this configuration (denoted LTO-G@Al, Scheme 1), due to the excellent electronic conductivity and flexible sheet structure of graphene, it forms an ultra-thin layer on the Al foil, which can significantly reduce the interface resistance and improve the adhesion and rate performance of LTO materials. The excellent electrochemical performance and very simple preparation of LTO-G@Al make it exceptionally suitable for high-rate LIBs.

## Experimental

***Preparation of electrode.***—Graphene prepared by the intercalation-exfoliation procedure[26] was received from Carbonene Technology Co., Ltd., Deyang, Sichuan, China. 7.5 g of graphene was dispersed in a solution of 2.5 g of polyvinylpyrrolidone (K30, Sinopharm Chemical Reagent Co., Ltd., China) and 0.3 g of carboxymethyl cellulose sodium (Sinopharm Chemical Reagent Co., Ltd., China) in 700 ml of deionized water by mechanical stirring to obtain the graphene slurry. The graphene slurry was pasted on an Al foil by a blade-coating method, and dried at 120°C for 24 h. The thickness of the graphene layer is about 2 μm, and this graphene coated Al foil was denoted as G@Al.

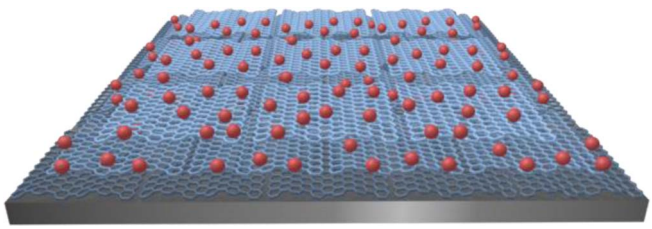

**Scheme 1.** Structural diagram of the LTO-G@Al electrode for LIBs.

[z]E-mail: fli@imr.ac.cn

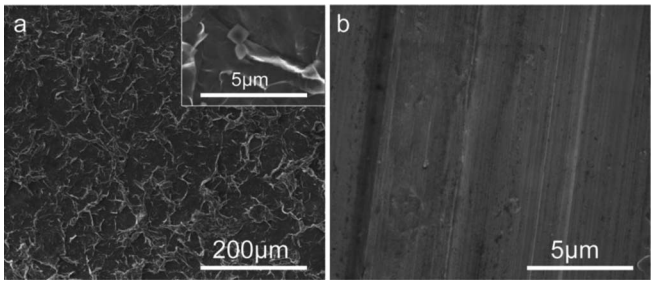


**Figure 1.** SEM images of (a) G@Al and (b) Al foil.

The active material slurry was prepared by mixing LTO powder (primary particle size is about 1 μm, Shenzhen BTR New Energy Materials Co., Ltd., China), carbon black (Super P, Timcal Ltd., Switzerland), and polyvinylidene fluoride (PVDF) binder (HSV-900, Arekma) in N-methyl-2-pyrrolidone (NMP) solvent. The weight ration of LTO: Super P: PVDF is 95:3:2. The slurry was then pasted onto surfaces of G@Al and Al foil and vacuum dried at 80°C for 24 h (denoted as LTO-G@Al and LTO@Al, respectively). After drying, the electrodes were pressed in a calendering machine. Typically, ∼7 mg of mixed powder was used for per coin cell. Afterward, they were calendered and punched into circular discs with a diameter of 12 mm and then pressed at 6 MPa for the subsequent electrochemical testing.

***Electrochemical characterization.—***Electrochemical tests were carried out in CR2025 coin-type cells using lithium metal as the counter/reference electrode and Celgard 2400 membrane as the separator. The electrolyte solution was 1 M $LiPF_6$ in a mixture of ethylene carbonate (EC) and dimethyl carbonate (DMC) (EC: DMC = 1: 1 v/v). Galvanostatic charge-discharge cycling test was performed on LAND CT2001A battery-testing system (Wuhan Land Electronics Co., China) at different rates (1 C corresponding to 175 mA $g^{-1}$) between 0.8 and 2.5 V vs. $Li/Li^+$ at room temperature. Electrochemical impedance spectroscopy (EIS) was carried out using a Solartron 1287/1260 electrochemical station. The amplitude of the AC signal was 5 mV over the frequency range of 0.01–$10^5$ Hz.

***Materials characterization.—***Scanning electron microscopy (SEM) were performed on FEI Nova NanoSEM 430. The sheet resistances of the electrodes with the current collectors were measured by a four-point method using a RTS-9 system (Guangzhou Four probes technology Co, China). The contact angles of the LTO slurry on the Al and G@Al were measured using an optical microscope. The adhesive strength between the LTO and the current collector was measured through a peeling test, using an electronic stress-strain tester (Instron 5567, UTM, USA).

## Results and Discussion

In this work, a graphene layer was fully covered on the Al surface by blade-coating, which plays an important role for improving the adhesion properties of Al foil. Graphene and LTO slurry were sequentially coated on Al foil. The morphology of both G@Al and Al foil surface was observed by SEM (Figure 1). Typically, the conventional Al foil has a relatively smooth surface with parallel scratches. In comparison, the G@Al foil is covered by graphene and is much rougher than that of Al.

Afterward, the wettability of G@Al and Al was evaluated by contact angle test using LTO slurry as shown in Fig. 2. As evidenced, the G@Al shows a contact angle of approximately 21° (Fig. 2a), which is much lower than that of Al (45°, Fig. 2b). It indicates that the G@Al can be much better wetted by the active material slurry than pristine Al foil. It is noted that the final layer on the Al foil is a composite layer contain graphene and PVP. First, graphene showed very good dispersion in NMP, which means strong affinity between graphene and NMP. Second, PVP is also a good binder to the polar

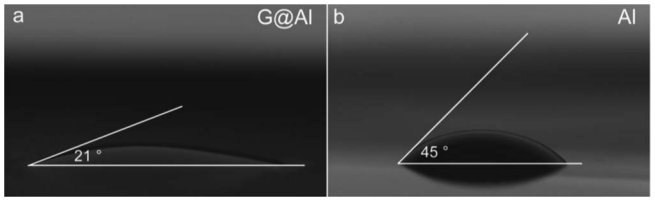


**Figure 2.** Contact angles of the LTO slurry on different current collectors. (a) LTO slurry on G@Al, (b) LTO slurry on Al.

surface, and thus could also contribute to the smaller contact angle. Third, NMP solvent in the LTO slurry is also a good solvent for PVP. Therefore, graphene and PVP comprehensively lead to the smaller contact angle of the LTO slurry on G@Al. Fig. 3 shows the cross-section of different pristine electrode, it can be seen that a 2–3 μm crack exists between the LTO layer and Al foil of the fresh LTO-Al electrode, while no such cracks were observed at the fresh LTO-G@Al interface (Fig. 3b), indicating a good contact between LTO and G@Al.

The adhesion between the current collector and active material also determines the electronic conductivity and the mechanical stability of the fabricated electrode.[27] To evaluate this, we characterized the interface adhesion by peel strength tests. The peeling curves of the LTO-Al and LTO-G@Al were shown in Fig. 4a. The slopes of peeling curves of the LTO-G@Al interface are much larger than those of the LTO@Al. This result clearly suggests a stronger interfacial binding of LTO-G@Al.[27]

For a good adhesion and mechanical stability of an electrode, the adhesion between binder and active materials should be high. Usually, carbon materials with high surface area, rich oxygen functional groups and porous structure show higher polymer absorption and better adhesion with binder.[28] And it is the wrinkled nature of the graphene layer and the better wetting at the LTO/graphene interface that collaboratively lead to the stronger adhesion between the LTO layer and the graphene coated current collector. The smaller contact angle indicates that G@Al shows a much lower surface tension, and stronger interface of LTO-G@Al has been formed.

Due to the strong interfacial binding between LTO and G@Al, the sheet resistance of LTO-G@Al can be significantly reduced in comparison with that of LTO@Al. As shown in Fig. 4b, the sheet resistance of LTO@Al was about 323.3 Ω/□ while the sheet resistance of LTO-G@Al was reduced by almost one order of magnitude to 33.5 Ω/□, which can be ascribed to the enhanced contact between LTO and graphene than that between LTO and Al. It is in agreement with the wettability results and can provide a much better electron transport between the current collect and the LTO.

To assess the influence of the graphene layer on the electrochemical performance of LTO based electrode, the as-prepared LTO-G@Al and LTO@Al were subsequently tested by galvanostatic charge-discharge cycling at different rates from 0.2 to 20 C (Fig. 5a). Both electrodes

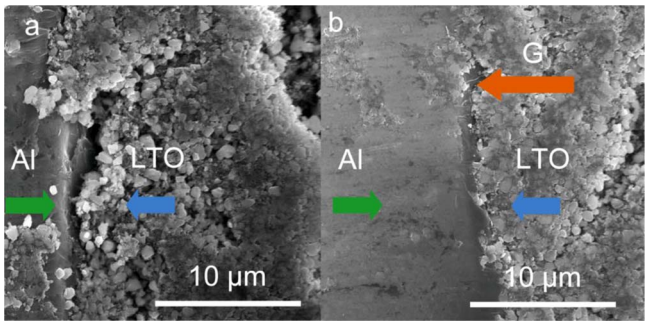


**Figure 3.** Cross-section of (a) LTO-Al and (b) LTO-G@Al electrodes before calendaring.

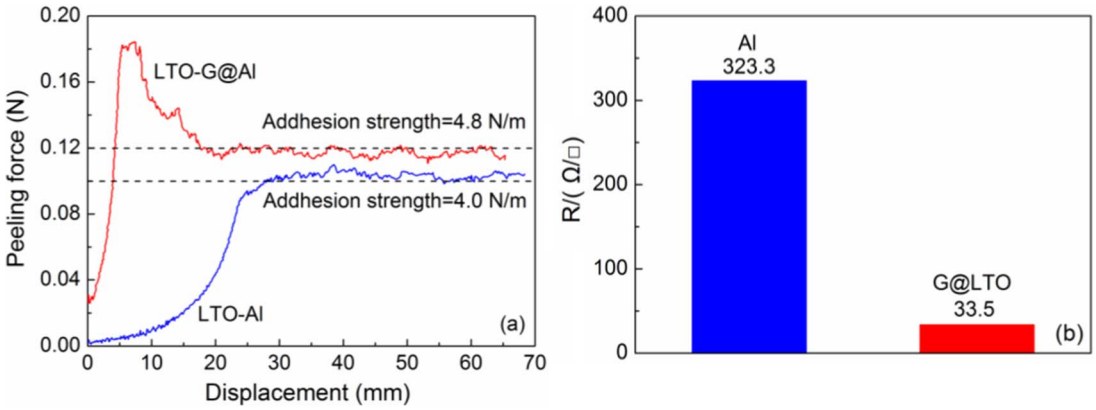


**Figure 4.** (a) Peeling curves of the LTO electrodes with different current collectors, (b) sheet resistance of LTO electrodes with different current collectors

exhibited similar specific capacities at low rates of 0.2 C, 0.5 C and 1 C. However, when tested at higher rates, it is noted that LTO-G@Al exhibited a much superior performance. Specifically, LTO-G@Al delivered 132.3 mAh/g, 111.8 mAh/g, 85.8 mAh/g and 54.8 mAh/g at 5 C, 10 C, 15 C, and 20 C. In comparison, the LTO@Al merely possessed a much lower capacity of 120.7 mAh/g, 78.6 mAh/g, 33.8 mAh/g and 9.35 mAh/g, respectively. Consequently, this graphene layer can significantly improve the rate performance of LTO electrodes, especially at extremely high rates.

The charge-discharge curves of the LTO-G@Al and LTO@Al electrodes were also obtained at these rates as shown in Figs. 5b, 5c. From these charge-discharge curves, it can be observed that both electrodes exhibit a flat operational potential plateau at relatively low rates, i.e. 1 C and 5 C. However, at higher rates, the potential plateau of the LTO@Al becomes shorter and gradually bends down while those of the LTO-G@Al electrode still remains flat. The potential margin between the charge and discharge plateaus can represent the degree of polarization of the electrode during the cycling. As shown in Figures 5b and 5c, the margin values of the LTO-G@Al electrode are much smaller than those of the LTO@Al electrode at all discharge rates. The margins of the plateau for LTO@Al electrode is 95.2 mV, 421.0 mV and 887.8 mV at 1 C, 5 C and 10 C, compared with 70.0 mV, 254.9 mV and 494.1 mV of LTO-G@Al, respectively. This suggests a much reduced polarization of the LTO-G@Al compared with LTO@Al, which is due to the better electronic and ionic conductivity from the graphene layer.

LTO-G@Al electrode also exhibits a better cycling performance than LTO@Al electrode as shown in Fig. 5d. After 50 cycles, the

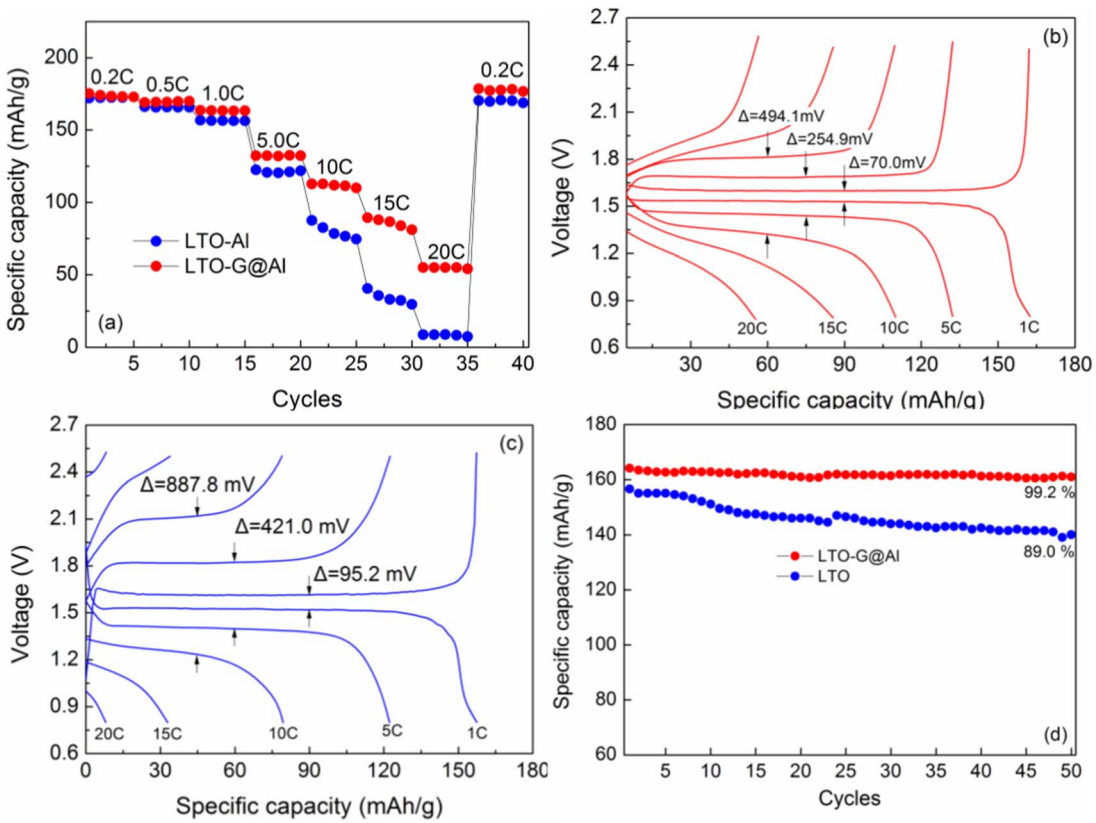


**Figure 5.** (a) Rate performance of LTO with different current collectors, (b) and (c) charge and discharge curves of 40 μm-thick-LTO electrodes with G@Al and Al current collectors, (d) cyclic performance of LTO with different current collectors.

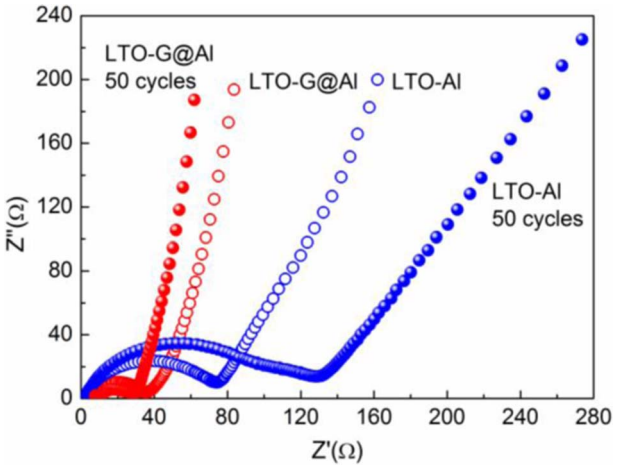


**Figure 6.** EIS spectra of LTO electrodes with different current collectors before and after 50 cycles.

capacity retentions of LTO-G@Al and LTO@Al were 99.2% and 89.0%, respectively. The better performance of LTO-G@Al can be ascribed to the stronger adhesion (Fig. 5), which is determined by electrochemical impedance spectra analysis before and after 50 cycles at 1 C.

The electrochemical procedures of both electrodes can be better revealed from their electrochemical impedance spectra (Fig. 6). The Nyquist plots of both electrodes consist of two overlapped and depressed semi-circle at high and middle frequency regions, as well as a straight line at low frequency. The semicircle at high frequency region represents the interface resistance ($R_{int}$), which can be attributed to (1) the contact resistance in the active layer, i.e. between LTO/carbon black particles, (2) the contact resistance between active material and current collector, (3) and/or the resistance of the passivating layer on the active materials. The middle frequency semicircle is due to the charge transfer resistance ($R_{ct}$), and the low frequency line is the characteristic of lithium ion diffusion inside the bulk electrode (Warburg).[29–32]

The width of this semi-circle gives the approximate overall charge transfer resistance ($R_{int}$ and $R_{ct}$). It was found that the LTO-G@Al has a significantly lower resistance than that of LTO@Al. More importantly, the resistance of LTO-G@Al was reduced to 29.1 Ω after 50 cycles, while that of LTO@Al increased to 129.4 Ω. The decreased resistance value is due to the improved contact between active materials and current collectors during cycling. These results are in good agreement with the galvanostatic charge-discharge and sheet resistances characterizations. Due to the similar experimental conditions of the two electrodes, such as the loading of LTO (6.2 ± 0.1 mg/cm$^2$) and other testing parameters, the observed difference in the resistance is apparently due to the existence of the coated graphene film.

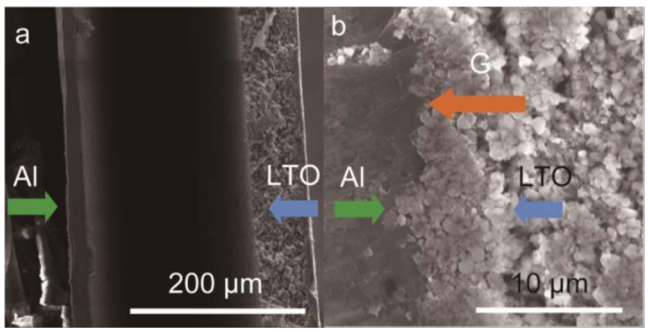


**Figure 7.** Cross-section of different cycled electrode (a) LTO-Al and (b) LTO-G@Al electrodes.

To better understand the influence of the graphene layer on the cycling stability of the electrodes, they were observed by SEM after being tested for 50 cycles. It can be observed, from the cross section of the electrodes, the LTO layer severely detached from the Al foil on the LTO@Al electrode (Fig. 7a), whilst the LTO layer was still closely adhered to the surface of G@Al on LTO-G@Al electrode (Fig 7b). This clear evident has again strongly proved the much better stability of LTO-G@Al compared with LTO@Al electrode.

## Conclusions

With the aim to solve the rate performance issue, we introduced a wrinkled graphene layer between the spinel $Li_4Ti_5O_{12}$ and the Al foil by a simple coating approach. This graphene layer provides a larger contact area, lower contact resistance, stronger adhesion between the active material and the current collector. As a result, the LTO material's rate performance and cycling stability has been significantly improved, without compromising its other characteristics. This low-cost graphene will not only greatly improve the performance but also shed light on the performance enhancement of other battery systems, such as a Li-sulfur battery or a Li-air battery.

## Acknowledgments

This work was supported by the Ministry of Science and Technology of China (2016YFA0200100, 2014CB932402), NSFC (Nos. 51521091, 51525206 and U1401243), "Strategic Priority Research Program" of the Chinese Academy of Sciences (XDA01020304).

## References

1. M. M. Thackeray, *J. Electrochem. Soc.*, **142**, 2558 (1995).
2. G. N. Zhu, Y. G. Wang, and Y. Y. Xia, *Energy Environ. Sci.*, **5**, 6652 (2012).
3. J. B. Goodenough, *Energy Storage Mater.*, **1**, 158 (2015).
4. A. S. Prakash, P. Manikandan, K. Ramesha, M. Sathiya, J. M. Tarascon, and A. K. Shukla, *Chem. Mater.*, **22**, 2857 (2010).
5. M. M. Rahman, J.-Z. Wang, M. F. Hassan, S. Chou, D. Wexler, and H.-K. Liu, *J.Power Sources*, **195**, 4297 (2010).
6. M. W. Raja, S. Mahanty, and M. Kundu, fand R. N. Basu, *J. Alloy. Compd.*, **468**, 258 (2009).
7. L. Cheng, X. L. Li, H. J. Liu, H. M. Xiong, P. W. Zhang, and Y. Y. Xia, *J. Electrochem. Soc.*, **154**, A692 (2007).
8. L. Cheng, J. Yan, G. N. Zhu, J. Y. Luo, C. X. Wang, and Y. Y. Xia, *J. Mate. Chem.*, **20**, 595 (2010).
9. R. Dominko, M. Gaberscek, A. Bele, D. Mihailovic, and J. Jamnik, *J. Eur. Ceram. Soc.*, **27**, 909 (2007).
10. L. Wen, Z. Y. Wu, H. Z. Luo, R. S. Song, and F. Li, *J. Electrochem. Soc.*, **162**, A3038 (2015).
11. D. Capsoni, M. Bini, V. Massarotti, P. Mustarelli, G. Chiodelli, C. B. Azzoni, M. C. Mozzati, L. Linati, and S. Ferrari, *Chem. Mater.*, **20**, 4291 (2008).
12. D. Capsoni, M. Bini, V. Massarotti, P. Mustarelli, S. Ferrari, G. Chiodelli, M. C. Mozzati, and P. Galinetto, *J. Phys. Chem. C*, **113**, 19664 (2009).
13. T. F. Yi, S. Y. Yang, and Y. Xie, *J. Mate. Chem. A*, **3**, 5750 (2015).
14. G. N. Zhu, H. J. Liu, J. H. Zhuang, C. X. Wang, Y. G. Wang, and Y. Y. Xia, *Energy Environ. Sci.*, **4**, 4016 (2011).
15. J. Gao, J. R. Ying, C. Y. Jiang, and C. R. Wan, *J. Power Sources*, **166**, 255 (2007).
16. K. Wang, S. Luo, Y. Wu, X. F. He, F. Zhao, J. P. Wang, K. L. Jiang, and S. S. Fan, *Adv. Funct. Mater.*, **23**, 846 (2013).
17. H. L. Pan, Y. S. Hu, H. Li, and L. Q. Chen, *Chin.Phys.B*, **20** (2011).
18. H. C. Wu, H. C. Wu, E. Lee, and N. L. Wu, *Electrochem. Commun.*, **12**, 488 (2010).
19. H. C. Wu, E. Lee, N. L. Wu, and T. R. Jow, *J. Power Sources*, **197**, 301 (2012).
20. K. Striebel, J. Shim, A. Sierra, H. Yang, X. Y. Song, R. Kostecki, and K. McCarthy, *J. Power Sources*, **146**, 33 (2005).
21. F. Y. Su, Y. B. He, B. H. Li, X. C. Chen, C. H. You, W. Wei, W. Lv, Q. H. Yang, and F. Y. Kang, *Nano Energy*, **1**, 429 (2012).
22. F. Y. Su, C. H. You, Y. B. He, W. Lv, W. Cui, F. M. Jin, B. H. Li, Q. H. Yang, and F. Y. Kang, *J. Mate. Chem.*, **20**, 9644 (2010).
23. N. Zhu, W. Liu, M. Q. Xue, Z. Xie, D. Zhao, M. N. Zhang, J. T. Chen, and T. B. Cao, *Electrochim. Acta*, **55**, 5813 (2010).
24. L. F. Shen, C. Z. Yuan, H. J. Luo, X. G. Zhang, S. D. Yang, and X. J. Lu, *Nanoscale*, **3**, 572 (2011).
25. Y. Shi, L. Wen, F. Li, and H. M. Cheng, *J. Power Sources*, **196**, 8610 (2011).
26. S. F. Pei, J. H. Du, F. Li, K. Huang, W. C. Ren, and H. M. Cheng, CN Pat. CN201110282370 (2011).
27. L. Wen, X. D. Hu, H. Z. Luo, F. Li, and H. M. Cheng, *Particuology*, **22**, 24 (2015).

28. M. E. Spahr, in *Lithium-ion batteries: Science and Technologies*, M. Yoshio, R. J. Brodd, and A. Kozawa, Editors, p. 135, Springer, Germany (2009).
29. J. Illig, M. Ender, T. Chrobak, J. P. Schmidt, D. Klotz, and E. Ivers-Tiffee, *J. Electrochem. Soc.*, **159**, A952 (2012).
30. M. Gaberscek, R. Dominko, and J. Jamnik, *J. Power Sources*, **174**, 944 (2007).
31. J. M. Atebamba, J. Moskon, S. Pejovnik, and M. Gaberscek, *J. Electrochem. Soc.*, **157**, A1218 (2010).
32. D. S. Lu, W. S. Li, X. X. Zuo, Z. Z. Yuan, and Q. M. Huang, *J. Phys. Chem. C*, **111**, 12067 (2007).